Virial Coefficients of Polarizable Water: Applications to Thermodynamic Properties and Molecular Clustering†

Kenneth M. Benjamin, Andrew J. Schultz, and David A. Kofke*

Department of Chemical and Biological Engineering, University at Buffalo, The State University of New York, Buffalo, New York 14260-4200

Received: June 4, 2007; In Final Form: August 20, 2007

We determine the second and third virial coefficients B_2 and B_3 for the Gaussian charge polarizable model (GCPM) as a function of temperature over the range 210−723 K. The overlap sampling implementation of Mayer sampling molecular simulation is applied to calculate the values, obtaining results to a precision that ranges from 0.1% for B_2 to an average of 1% for B_3. These calculated values compare very well with known values of B_2 and B_3 for real water and outperform both pairwise models and other polarizable models in describing experimental virial-coefficient data. We examine these coefficients in the context of the equation of state and molecular clustering. Comparisons are made to established molecular simulation data, quantum chemical calculations, and experimental data for real water. Under both saturated-vapor and supercritical conditions, the virial series up to B_3 describes the equation of state quite well. The virial coefficients are used to characterize molecular clusters (dimers and trimers) in GCPM water under supercritical, saturated vapor, and atmospheric conditions between 210−673 K. The analysis shows that the extent of clustering in polarizable water is diminished relative to that from a pairwise water model.

1. Introduction

The virial equation of state (VEOS)[1,2] plays an important role in our understanding the pressure−volume-temperature (*PVT*) behavior of gases. The VEOS describes the *PVT* behavior at low density by the following expression:

$$\frac{P}{\rho kT} \equiv Z = 1 + B_2\rho + B_3\rho^2 + B_4\rho^3 + B_5\rho^4 + B_6\rho^5 + \ldots \quad (1)$$

Here P is the pressure, ρ is the number density (reciprocal of volume per molecule, v), k is the Boltzmann constant, T is the absolute temperature, Z is the compressibility factor, and B_i is the ith virial coefficient. These coefficients are directly related to the interactions between the molecules. The first term on the right-hand side in the above equation (the constant 1) represents the ideal-gas contribution, and subsequent terms represent the contributions from many-body interactions as found in real (that is, nonideal) systems. In particular, B_i is related to interaction energies of a group of i molecules. These coefficients often are represented in the form of cluster diagrams.[2,3] For example:

$$B_2(T) = -\frac{1}{2V}$$ 

where V is the volume. For the third virial coefficient:

$$B_3(T) = -\frac{1}{3V}$$ 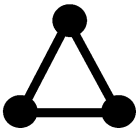

In the diagrams the points correspond to a variable of integration (such as positions, or distance between molecules) and the lines represent Mayer function interactions $\{f_{ij} = [\exp(-\beta u_{ij}) - 1]$, where u_{ij} is the pair potential between molecules labeled i and j, and $\beta = (kT)^{-1}\}$ between the molecules. We do not include here the symmetry number in the definition of the diagram, but instead we make it an explicit part of the multiplying coefficient.

Virial coefficient data for realistic potentials are scarce. Recently, we introduced Mayer sampling, a method based on free energy perturbation ideas applied to the calculation of cluster integrals.[4−6] Using this method, we calculated up to B_6 for Lennard-Jones fluid (LJ)[4,5] and a host of pairwise water models.[6] Additionally, virial coefficients up to B_4 for two-centered Lennard-Jones with quadrupole (2CLJQ)[7] and B_3 for the polarizable point charge (PPC) water model[8] have been determined using other methodologies, such as numerical integration[8] and the hit-and-miss Monte Carlo (MC) method.[9]

In the present study, we apply the Mayer sampling method to calculate B_2 and B_3 for the Gaussian charge polarizable model (GCPM) of Paricaud et al.[10] This model was developed by fitting to experimental data for the microstructure of ambient liquid water and vapor−liquid equilibria. Virial-coefficient data were not used in its formulation, so the present study provides a useful test of the model. All calculations performed here are classical, and contain no quantum-mechanical corrections. This approach is appropriate to the model, inasmuch as GCPM is an empirical potential with parameters fitted to experimental data, and hence it implicitly contains quantum mechanical effects.[11] Using the calculated virial coefficients, we investigate the *PVT* behavior and molecular clustering of this model. The rest of the paper is organized as follows. In the next section, we review the mathematical formalism for calculating virial coefficients for systems with nonadditive intermolecular forces. In Section 3, we present the polarizable water model studied herein and briefly describe the Mayer sampling technique. In Section 4, we present

† Part of the "Keith E. Gubbins Festschrift".

* Corresponding author. Telephone: (716) 645-2911 ext. 2215. Fax: (716) 645-3822. E-mail: kofke@buffalo.edu.

10.1021/jp0743166 CCC: $37.00
Published on Web 10/11/2007

virial coefficients B_2 and B_3 for the GCPM and discuss thermodynamic properties and molecular clustering predicted from the third-order virial equation of state. It should be noted that this is the first calculation of B_2 and B_3 for GCPM water. Finally, we conclude in Section 5.

2. Virial Coefficients for Nonpairwise Potentials

While potential models such as Lennard-Jones and square-well are defined by pairwise interactions, such is strictly not the case for real fluids. This is particularly true for a polarizable fluid like water. While much effort has gone into the development of empirical pairwise potentials for liquid water (such as SPC/E[31] and TIP4P[34]), these pairwise models, though computationally convenient, often fail to describe the properties of water vapor accurately. They were formulated to emphasize accurate description of the liquid phase, and because they are not polarizable, they cannot describe behavior over a broad range of densities; consequently, the vapor-phase performance suffers. This fact is especially evident for virial coefficients. As Kusalik et al. showed in the calculation of B_3 for water, a polarizable potential like the polarizable point charge (PPC) model outperforms the most commonly used pairwise potentials, SPC/E and TIP4P.[8] In our previous Mayer sampling investigation,[6] we established that none of the standard pairwise models for water (viz. SPC,[30] SPC/E,[31] MSPC/E,[32] TIP3P,[33] and TIP4P[34]) were capable of reproducing B_2 within 20% for real water below a temperature of about 700 K.

To compute the virial coefficients of polarizable water correctly, we require a formalism that accounts for the nonadditivity of the intermolecular forces. Johnson and Spurling provide such a formalism.[12] The third virial coefficient, B_3, is represented as the sum of additive and nonadditive parts, as in

$$B_3(T) = B_{3,\mathrm{add}} + \Delta B_3 \tag{4}$$

where the pairwise additive component is of the standard form

$$B_{3,\mathrm{add}} = \frac{-1}{3}\left\langle \int\int f_{12}f_{13}f_{23}\,\mathrm{d}\mathbf{r}_{12}\,\mathrm{d}\mathbf{r}_{13}\right\rangle_{\Omega_1\Omega_2\Omega_3} \tag{5}$$

in which the factor of V is cancelled by integrating over the positions of molecule 1 and taking it as the origin for subsequent integrals, as indicated. These types of integrals are commonly referred to as cluster integrals.[2,3] The nonadditive term for B_3 is

$$\Delta B_3 = \frac{-1}{3}\left\langle \int\int\left[\exp\left(\frac{-\Delta u_{123}}{kT}\right)-1\right]\times \exp\left(\frac{-\{u_{12}+u_{13}+u_{23}\}}{kT}\right)\mathrm{d}\mathbf{r}_{12}\,\mathrm{d}\mathbf{r}_{13}\right\rangle_{\Omega_1\Omega_2\Omega_3} \tag{6}$$

where the Δu_{123} term equals the difference between the actual trimer energy and the sum of the pair energies:

$$\Delta u_{123} = u_{123} - (u_{12}+u_{13}+u_{23}) \tag{7}$$

and $\Omega_1\Omega_2\Omega_3$ indicates averaging the integral over all orientations of the three respective water molecules.

3. Computational Details

This section presents the specific water model studied and the Mayer sampling method itself. Particular attention is focused on the use of overlap sampling.

3.1. Gaussian Charge Polarizable Model for Water. In this investigation, we apply the Mayer sampling method to calculate values of B_2 and B_3 for the Gaussian charge polarizable model for water developed by Paricaud et al.[10] The key features of this potential model are an exponential-6 representation of dispersion interactions and the representation of partial charges by spherical Gaussian charge distributions. These features allow the GCPM to successfully describe the microstructure of liquid water, vapor−liquid equilibrium, thermodynamic properties, transport properties, and even water dimer energies.

It should be noted that as the GCPM is polarizable, its electrostatics must be solved self-consistently for each configuration. As outlined in the literature,[10] the electric fields on each molecule and induced dipoles of each molecule are resolved simultaneously by iteration of the induced dipoles. The criterion we employed for convergence was a change in the induced dipole (on each molecule) of less than 1.3×10^{-17} Debye. Typically, 3−5 iterations were required for a B_2 simulation, while 7−10 were required for B_3. With so few molecules the polarization can alternatively be solved by direct inversion of the field equations, but we did not employ such an approach in this work.

The Mayer sampling method (described in the next section) is performed in an infinite volume with no periodic images or other containing structures. Thus, except as described below, there is no truncation of the potential, and no Ewald sum or other long-range correction needs to be applied in the calculation.

3.2. Mayer Sampling. The Mayer sampling method[4−6] was recently introduced for evaluation of the integrals appearing in the expressions for the virial coefficients. A complete description of the method exists elsewhere in the literature,[6] so what follows is just a brief outline.

Mayer sampling is a Monte Carlo approach that adopts ideas used for the evaluation of free energies.[13,14] Molecular configurations are sampled using importance sampling with weights based on the magnitude of the interactions that are represented in the given cluster integral. Simulation averages give the ratio of the desired cluster integral to that of a known reference integral, as follows:

$$\Gamma(T) = \Gamma_0\frac{\Gamma}{\Gamma_0} = \Gamma_0\frac{\langle\gamma/\pi\rangle_\pi}{\langle\gamma_0/\pi\rangle_\pi} \tag{8}$$

where $\Gamma(T)$ represents a general cluster integral or sum of integrals, $\gamma(\mathbf{r^n}, T)$ is the integrand (or sum of integrands), and $\pi(\mathbf{r^n}, T) = |\gamma|$ is the unnormalized probability distribution that governs sampling. The angle brackets indicate the "ensemble-average" integral over all configuration space. Quantities marked with the subscript "0" correspond to the specified reference system, for which a hard-sphere model provides a suitable choice.

Equation 8 corresponds to a direct sampling method, as it involves perturbations directly between the target system (which governs sampling) and the reference system. At low temperatures the water molecules strongly prefer their own energetic wells, and many configurations important to the hard sphere reference are not sampled, and direct sampling fails. This signals that the hard-sphere phase space is no longer a subset of the water phase space[13,14] but instead that the water's attractive wells are regions of phase-space overlap between the hard spheres and water. Overlap sampling is a desirable alternative to direct sampling in such situations.

The main idea behind overlap sampling is to sample two separate systems (one with the sampling governed by the water

TABLE 1: Negligible Effect of Transition Distance (to Pairwise Interactions) on B_3 for GCPM Water at 546 K (10^9 Samples)

transition (Å)	B_3 (L/mol)^2
100	−0.00300(3)
200	−0.00301(4)

potential and the other governed by the hard sphere potential), with each perturbing into a common intermediate. This intermediate is designed to contain important configurations from the intersection of the individual configurations of the two original systems. One begins by defining an overlap function to represent mathematically only those regions important to both hard spheres and water:

$$\gamma_{OS} = \frac{|\gamma_0||\gamma|}{\alpha|\gamma_0| + |\gamma|} \tag{9}$$

where γ_{OS} is the overlap function and α is an optimization parameter. In each phase, the quantity measured during the simulation is the ratio of the average value of the cluster to the average overlap function for that system. The ratio of the water to the hard-sphere integrals can then be calculated as the ratio of the ratios from the hard-sphere and water systems:

$$\Gamma(T) = \Gamma_0 \frac{\langle \gamma/\pi \rangle_\pi / \langle \gamma_{OS}/\pi \rangle_\pi}{\langle \gamma_0/\pi_0 \rangle_{\pi_0} / \langle \gamma_{OS}/\pi_0 \rangle_{\pi_0}} \tag{10}$$

where $\pi_0 = |\gamma_0|$. The parameter α and the amount of sampling performed for each system can be selected to optimize the calculation.[6]

One important feature of these simulations for polarizable water is that at a certain distance, the potential interactions were forced to be pairwise additive (rather than nonadditive) when evaluating the cluster integrals for coefficients B_3. The computational necessity of this transition can be seen from considering the following. In the case of B_3, there are three water molecules present in the simulation, and the solution requires the self-consistent resolution of the electric fields and induced dipole moments of all three molecules. For instances when two molecules are close together and the third a large distance away, the effect of the third water molecule is not so much to add to the energy of the trimer (relative to the energy of the dimer pair close together), but rather to alter the electric fields and induced dipoles felt by the first two molecules, which are in close proximity. At these large separations (between the pair of molecules and the third), it becomes increasingly difficult to resolve the electric fields within machine precision during the iterative solution. To circumvent this problem, we elected to force the interactions to be pairwise (which is the limiting behavior at infinite distances) before this difficulty in solution closure became unmanageable. The distance chosen for the B_3 simulations was 100 Å. To demonstrate that there are no adverse effects from this practice, we present in Table 1 values of B_3 at 546 K determined from simulations with transitions to pairwise interactions at 100 and 200 Å, respectively. As the results show, the values determined with the two different transition distances agree within their uncertainties. This allows us to proceed with confidence in using the 100-angstrom transition for the B_3 simulations.

For B_2 at all temperatures and B_3 between 210 and 600 K, 10^9-10^{10} samples were required to obtain a low uncertainty (usually ≤1%). For B_3 between 600 and 723 K, 10^{10} configurations were sampled and provided uncertainties less than 3%.

TABLE 2: Virial Coefficients for GCPM Water[10] As Calculated Using the Mayer Sampling Method[a]

T (K)	B_2 (L/mol)	B_3 (L/mol)^2
210	−12.42(1)	$-1.72(2) \times 10^4$
230	−5.975(4)	$-1.64(1) \times 10^3$
250	−3.304(4)	−254(1)
270	−2.036(3)	−53.6(2)
290	−1.362(5)	−14.60(5)
298	−1.1765(8)	−9.20(3)
331	−0.7094(6)	−1.786(5)
350	−0.556(1)	−0.810(2)
373	−0.4307(4)	−0.3424(9)
400	−0.3301(4)	−0.1402(4)
420	−0.276(1)	−0.0775(2)
438	−0.2405(3)	−0.0466(2)
456	−0.2100(6)	−0.0287(1)
474	−0.1860(4)	−0.0183(1)
492	−0.1649(5)	−0.0116(1)
510	−0.1476(3)	−0.00739(5)
528	−0.1330(3)	−0.00483(4)
546	−0.1202(3)	−0.00300(3)
564	−0.1086(3)	−0.00179(3)
582	−0.0994(2)	−0.00104(2)
590	−0.0953(2)	−0.00073(2)
600	−0.0911(4)	−0.000505(4)
610	−0.0864(2)	−0.000282(8)
642.21[b]	−0.0744(2)	0.000156(6)
648	−0.073(1)	0.000224(7)
673	−0.0646(4)	0.000376(6)
723	−0.0523(5)	0.00051(1)

[a] Numbers in parentheses represent the confidence limits (standard error of the mean) for the rightmost digits of the value. [b] Critical temperature.

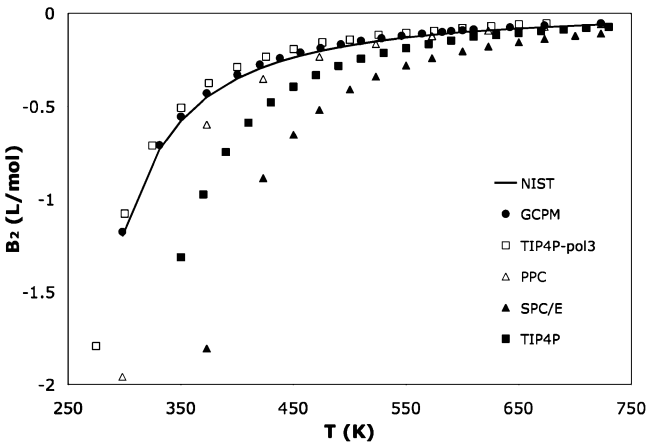

Figure 1. Comparison of second virial coefficient from various water models. Points are Mayer sampling results for each corresponding model, and lines are results from a correlation for real water.[15]

For each virial coefficient at each specific temperature, an average was calculated and the standard error of the mean was computed from the respective block averages, and is reported with the results.

4. Results and Discussion

4.1. Virial Coefficients. Table 2 presents the virial coefficients B_2 and B_3 for GCPM water studied in this work. As was shown for pairwise water models,[6] the general trend for both virial coefficients is to tend from negative to positive values as temperature increases. To better assess the quality of these results, it is instructive to compare them to virial coefficients reported for other water models (both pairwise and polarizable) and for real water. Figure 1 compares values for B_2. The line represents values from a highly accurate correlation for real

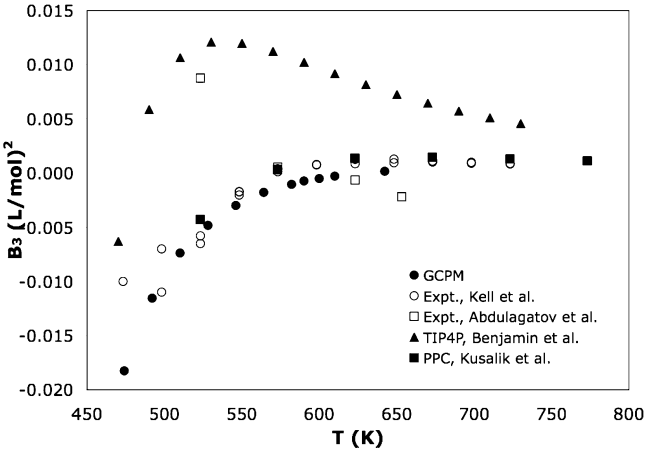

Figure 2. Comparison of third virial coefficient from various water models. Closed symbols are calculated results for each corresponding model, and open symbols are experimental results for real water.

water[15] and the symbols are results from various water models from various sources[6,8,16] and from this investigation. As the figure displays, GCPM water outperforms the best[6] pairwise water models (SPC/E[31] and TIP4P[34]), a simple polarizable water model (PPC[8]), and a more advanced polarizable water model (TIP4P-pol3[16]). The agreement between GCPM water and real water is excellent over a wide range of temperatures.

In Figure 2, we compare values of the third virial coefficient, B_3, for GCPM water with previous calculations[6,8] and with experimental values for real water.[17,18] As in the case of B_2, B_3 values for GCPM water agree better with values for real water than do those of the best pairwise model, TIP4P (discounting what appears to be a spurious outlying datum from Abdulagatov et al.). Again, the overall agreement between GCPM water and the experimental investigations is exceptional. Over the temperature range displayed in Figure 2, 450−800 K, GCPM water seems to perform equally well as PPC water. However, if one considers B_3 at 373 K, the GCPM produces a value of B_3 equal to −0.3424 (L/mol),^{2} while the PPC water model predicts a value of −0.627 (L/mol).[28] If one recalls that B_2 for PPC water began to deviate significantly from that of real water at 423 K and below (see Figure 1), one should expect similar, or worse, agreement between B_3 for PPC water and real water at 423 K and below.

4.2. Thermodynamic Properties. Having determined virial coefficients B_2 and B_3 for GCPM water, we now turn our attention to calculating thermodynamic properties via the virial equation of state (VEOS) truncated at the third order. The first comparison we make is for saturated water vapor along the coexistence curve, which represents the highest density of interest for the subcritical vapor. Here, we compare the deviation from ideality, $(Z - 1)$ [where Z is the compressibility factor, $Z = P/\rho RT$], for GCPM water as determined from various truncated VEOS to values determined from Gibbs ensemble Monte Carlo (GEMC) simulations with GCPM water.[10] In making this comparison, we use the saturation temperature and the vapor density for the model (as determined from GEMC) as input to the VEOS, and compute the saturation pressure. This, in turn, can be used to compute the quantity $(Z - 1)$. It should be noted that temperature varies in this comparison, increasing with the saturation density.

Figure 3 displays the deviations from ideality as a function of saturated vapor density for the GEMC results as well as virial equations of state truncated at the second and third orders (VEOS2 and VEOS3, respectively). The figure shows that the

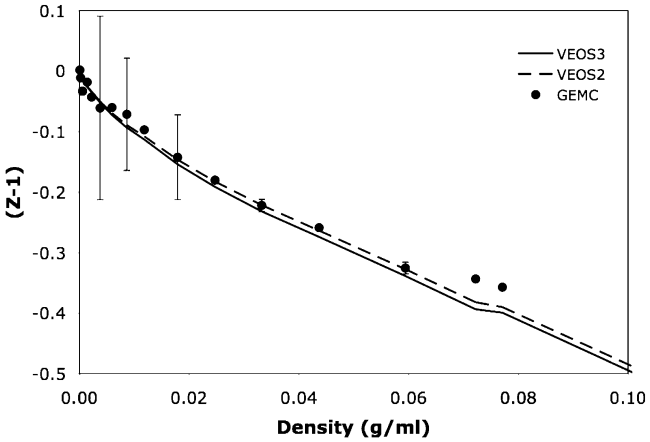

Figure 3. Deviation from ideality along the saturated vapor line of GCPM water. Solid line is VEOS3, dashed line is VEOS2, and points are molecular simulation data from Paricaud et al.[10]

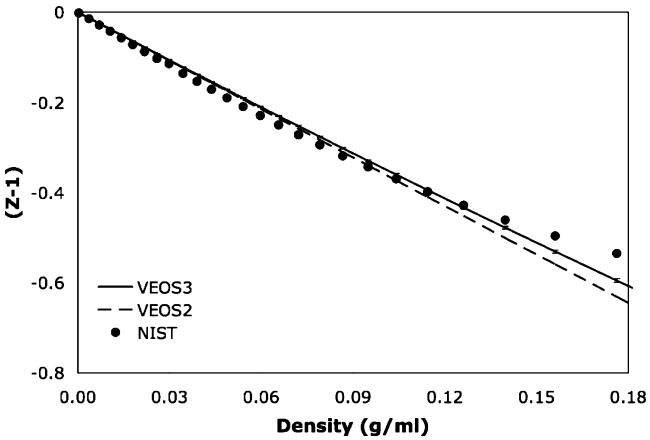

Figure 4. Deviation from ideality for supercritical GCPM water[10] at 673 K. Solid line is VEOS3, dashed line is VEOS2, and points are results from a highly accurate equation of state for real water.[19]

difference between VEOS2 and VEOS3 is small over this density range, and both equations agree well with GEMC results to a density of about 0.06 g/mL. Resolution of the discrepancy beyond this point requires knowledge of higher-order coefficients.

In Figure 4, we compare the deviations from ideality of VEOS3 and VEOS2 for GCPM water with a highly accurate equation of state for real water[19] under supercritical conditions. Figure 4 displays results at 673 K and indicates that VEOS3 is accurate up to a density of around 0.15 g/mL. This comparison suggests that VEOS3 for GCPM water is a suitable equation of state for modeling the pressure−volume-temperature of real supercritical water, out to roughly half the critical density.

4.3. Molecular Clustering. In this section, we examine the phenomenon of molecular clustering as understood through virial coefficients. Molecular clusters are aggregates of molecules that exist as discrete entities either due to chemical/energetic interactions, such as hydrogen bonds, or physical interactions—that is, the individual molecules are in close proximity to one another without any significant energetic relationship. In the virial analysis, two or more molecules constitute a cluster if they interact in a way that affects the thermodynamic properties of the bulk fluid, as described by the virial equation of state. The virial coefficient method for describing clustering was first presented by Woolley[20] and has been expanded to higher-order virial coefficients recently by Benjamin et al.[21] In this section, we will examine clustering under three different conditions: supercritical, subcritical saturated vapor, and atmospheric.

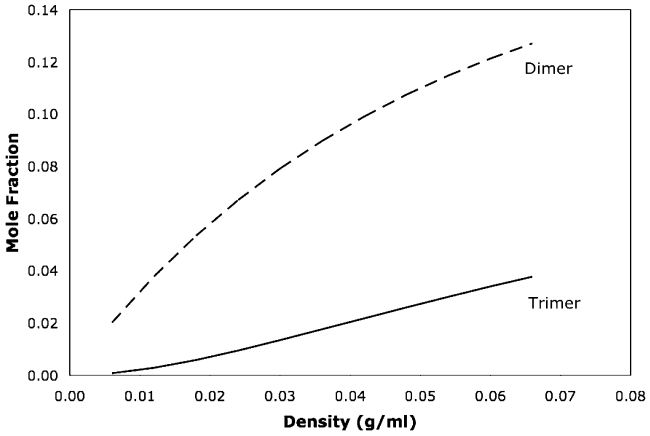

Figure 5. Mole fraction of dimer and trimer water clusters for supercritical GCPM water[10] at 673 K.

TABLE 3: Average Cluster Sizes in Supercritical Water at a Reduced Temperature (T/T_c) of 1.04, Showing Pairwise vs Polarizable Water Models, Where Reduced Density ρ_r Is the Density Divided by the Critical Density

	⟨S⟩		
ρ_r	TIP4P[34]; Monte Carlo[25]	TIP4P[34]; virial coeffs[21]	GCPM[10]; virial coeffs
0.06	1.15	1.14	1.07
0.15	1.39	1.33	1.17

4.3.1. Supercritical Conditions. Chemistry in supercritical water is an area of research that is concerned greatly with the cluster composition of water. The extent of water clustering can affect the solvation of various reactants, transition states, and products during elementary reactions.[22] Also, different water clusters (dimers, trimers, etc.) could become potential reactants and provide alternative reaction pathways. In addition, the clustering is a function of the thermodynamic state (temperature and pressure) of the water.[23−25] A thorough knowledge of the cluster composition is helpful in understanding the structure of the local molecular environment, deducing the fundamental reaction mechanism and energetics, and selecting appropriate reaction conditions.

The problem of molecular clustering in supercritical water has been studied previously.[21,23−25] In particular, Benjamin et al. compared clustering in supercritical TIP4P water via the virial coefficient approach to the conventional Monte Carlo results for TIP4P water obtained by Kalinichev and Churakov.[25] Table 3 contains two comparisons of clustering in supercritical water at a reduced temperature (T/T_c) of 1.04. The first comparison is between columns two and three, which shows that for a common water model (TIP4P in this case) the virial coefficient approach yields equivalent average cluster sizes when compared to conventional Monte Carlo simulation results. The second comparison is between columns three and four, which indicates that the extent of clustering is diminished in a polarizable water model relative to a pairwise water model. The fact that the pairwise water models (like TIP4P) overpredict the degree of clustering is due to the fact that the pairwise models were parametrized for liquid water, and therefore overestimate the amount of polarization that occurs in the gas phase. It should be noted that the clustering analysis is made only for conditions where the VEOS gives a good description of the equation of state for the water model of interest.

Figure 5 shows more detailed information about clustering for supercritical GCPM water. At 673 K, there is significant formation of dimers, and non-negligible formation of trimers under supercritical conditions at densities less than 0.07 g/mL.

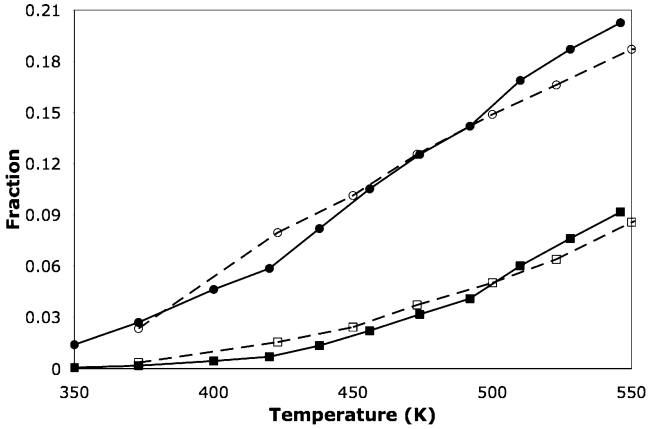

Figure 6. Fraction of water molecules in clusters in the vapor phase along the coexistence curve of water: GEMC simulations[26] with SPC/E[31] water (H-bonded clusters) vs virial-clustering approach with GCPM water.[10] Key: (●) dimer, virial/GCPM; (○) dimer, GEMC/SPCE; (■) trimer, virial/GCPM; (□) trimer, GEMC/SPCE.

4.3.2. Saturated Vapor Conditions. Next we consider clustering at states located along the vapor−liquid coexistence curve. Johansson et al.[26] performed GEMC simulations of the SPC/E model for water and analyzed clusters that formed in the vapor phase. Their results can be compared to the virial-coefficient approach to cluster characterization, using the newly determined values of B_2 and B_3 for GCPM water. Figure 6 shows this comparison, and presents the fraction of molecules that are present in a cluster of size n, for n equal to 2 (dimer) and 3 (trimer). (One should note in examining Figure 6 that the quantities plotted are not the cluster fractions, but the fraction of atoms in a cluster of a given size; this measure gives greater weight to the larger clusters.) With the exception of temperatures above 500 K, the fractions for $n = 2$ and $n = 3$ given by the virial approach are slightly lower than those counted by GEMC simulations. This finding is consistent with that in the supercritical water case, which is that clustering in polarizable water, as a whole, is reduced relative to that of pairwise water. The differences between the results for SPC/E and GCPM water in Figure 6, including the larger cluster fractions for GCPM above 500 K, can be understood best by considering several factors. The first is that the SPC/E and GCPM water models inherently are different, and would be expected to produce different results. Additionally, these sets of clustering data differ due to the types of clusters being counted. The detailed data reported by Johansson et al. consider only hydrogen-bonded clusters, and thus exclude clusters that are physically associated but not hydrogen-bonded. In comparison, the virial coefficient approach counts both chemical (hydrogen-bonded) and physical clusters. So the physical, or total, number of clusters for SPC/E water would be noticeably larger than the reported fractions for chemical clusters at each respective saturation temperature. Even further, at higher temperatures hydrogen-bonding association is diminished relative to physical association, and the GEMC simulations will overlook even more clusters that are counted in the virial approach. This also may explain some of the discrepancy between the GEMC and the virial results as temperature increases. (In both approaches. the cluster fraction still increases because the density is increasing with temperature along the saturation line.)

It should be noted that the clustering analysis was based upon conditions where VEOS3 successfully described the thermo-

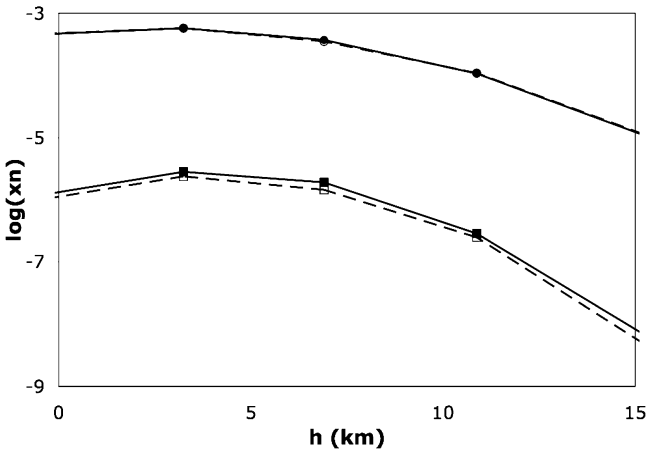

Figure 7. Mole fraction of water clusters in the atmosphere: Histogram Reweighting Monte Carlo (HRMC) simulations with TIP4P-pol3 water[16] vs virial-clustering approach with GCPM water. Key: (●) dimer, virial/GCPM; (○) dimer, HRMC/TIP4P-pol3; (■) trimer, virial/GCPM; (□) trimer, HRMC/TIP4P-pol3.

TABLE 4: Comparison of Water Cluster Concentrations in Saturated Air at 298 K with $P^{vap}(H_2O) = 0.031$ atm, Showing the Computational Quantum Chemistry[29] vs Virial Coefficient Method for GCPM Water[10]

	cluster concentration (clusters/cm^3)	
cluster	from ab initio/DFT	from virial coeff
dimer	9.0×10^{14}	1.1×10^{15}
trimer	2.6×10^{12}	9.0×10^{12}

dynamics of the saturated vapor phase and provided a good fit to GEMC results for GCPM water under saturated vapor conditions[10] (see Figure 3).

4.3.3. Ambient Conditions. Another area of research heavily interested in water clusters is atmospheric chemistry. It has long been speculated that water clusters may be abundant in atmospheric systems and may play important roles in physical and chemical processes contributing to global warming.[27,28] Dunn et al.[29] attempted to quantify the concentrations of water clusters up to pentamers in the atmosphere via computational quantum chemistry, which necessarily treats only chemically associated clusters. Table 4 compares the results of Dunn et al. with cluster concentrations calculated from GCPM virial coefficients for water vapor in saturated air at 298 K. The dimer concentrations given by the two approaches differ by only 20%, and the trimer concentrations differ by a factor of 3−4. For each respective cluster, the virial-based GCPM values are larger than the DFT values. These discrepancies with Dunn et al. must be ascribed to the difference between chemical and physical association (as DFT calculations count only chemical, while the virial approach counts both), with the conclusion that there are roughly 20% more physically associated pairs of water molecules than those that are associated by hydrogen bonding.

An additional investigation worth comparing to is the work of Chen et al.[16] who studied atmospheric water clustering using histogram reweighting Monte Carlo (HRMC) methods. Chen et al. calculated water cluster compositions for various empirical water force fields, including the highly accurate polarizable TIP4P-pol3 model, for temperatures and pressures corresponding to elevations ranging from sea level to 15 km. Figure 7 displays the HRMC results of Chen et al. for TIP4P-pol3 and the virial-clustering results for GCPM water. As the figure shows, both methods agree in their predictions of dimer and trimer compositions. This agreement validates both the GCPM water model and the virial clustering approach, especially in the limit of low density.

5. Conclusions

Mayer sampling molecular simulation is used to determine values for B_2 and B_3 for GCPM water. The data are in very good agreement with experimental B_2 and B_3 data for real water, which is a true credit to the GCPM as a water model, as it was not fit with any explicit consideration of the virial coefficients. The virial coefficients are then used in the virial series to predict *PVT* properties of saturated vapor-phase water and supercritical water, and the extent of molecular clustering in supercritical water, saturated water vapor, and in the atmosphere. Overall, the virial equation of state truncated at B_3 does a good job describing sub- and supercritical water. As a whole, the extent of clustering in polarizable water is less than that indicated by a pairwise water model.

Acknowledgment. Funding for this research was provided by Grant CTS-0414439 from the U.S. National Science Foundation.

References and Notes

(1) Reed, T. M.; Gubbins, K. E. *Applied Statistical Mechanics*; McGraw-Hill: New York, 1973.

(2) Mason, E. A.; Spurling, T. H. The Virial Equation of State. *The International Encyclopedia of Physical Chemistry and Chemical Physics, Topic 10: The Fluid State, Volume 2*; Pergamon Press Ltd.: Oxford, U.K., 1969.

(3) McQuarrie, D. A. *Statistical Mechanics*; University Science Books: Sausalito, CA, 2000. Gray, C. G.; Gubbins, K. E. *Theory of Molecular Fluids. Volume 1: Fundamentals*; Oxford University Press: London, 1984.

(4) Singh, J. K.; Kofke, D. A. *Phys. Rev. Lett.* **2004**, *92*, Art. No. 220601.

(5) Singh, J. K.; Kofke, D. A. *Phys. Rev. Lett.* **2005**, *94*, Art. No. 249903.

(6) Benjamin, K. M.; Singh, J. K.; Schultz, A. J.; Kofke, D. A. Higher-Order Virial Coefficients of Water Models. *J. Phys. Chem. B* **2007**, *111*, 11463.

(7) MacDowell, L. G.; Menduina, C.; Vega, C.; de Miguel, E. *J. Chem. Phys.* **2003**, *119*, 11367.

(8) Kusalik, P. G.; Liden, F.; Svishchev, I. M. *J. Chem. Phys.* **1995**, *103*, 10169.

(9) Ree, F. H.; Hoover, W. G. *J. Chem. Phys.* **1964**, *40*, 939.

(10) Paricaud, P.; Predota, M.; Chialvo, A. A.; Cummings, P. T. *J. Chem. Phys.* **2005**, *122*, 244511.

(11) Wick, C. D.; Schenter, G. K. *J. Chem. Phys.* **2006**, *124*, 114505.

(12) Johnson, C. H. J.; Spurling, T. H. *Aust. J. Chem.* **1974**, *27*, 241.

(13) Kofke, D. A. *Fluid Phase Equilib.* **2005**, 228−229C, 41.

(14) Kofke, D. A.; Frenkel, D. In *Handbook of Molecular Modeling*; Yip, S., Ed.; Springer, Dordrecht, the Netherlands 2005; p 683.

(15) Harvey, A. H.; Lemmon, E. W. *J. Phys. Chem. Ref. Data* **2004**, *33*, 369.

(16) Chen, B.; Siepmann, J. I.; Klein, M. L. *J. Phys. Chem. A* **2005**, *109*, 1137.

(17) Kell, G. S.; McLaurin, G. E.; Whalley, E. *J. Chem. Phys.* **1968**, *48*, 3805.

(18) Abdulagatov, I. M.; Bazaev, A. R.; Gasanov, R. K.; Ramazanova, A. E. *J. Chem. Thermodyn.* **1996**, *28*, 1037.

(19) http://webbook.nist.gov/chemistry/fluid.

(20) Woolley, H. W. *J. Chem. Phys.* **1953**, *21*, 236.

(21) Benjamin, K. M.; Schultz, A. J.; Kofke, D. A. *Ind. Eng. Chem. Res.* **2006**, *45*, 5566.

(22) Akiya, N.; Savage, P. E. *Chem. Rev.* **2002**, *102*, 2725.

(23) Mountain, R. D. *J. Chem. Phys.* **1999**, *110*, 2109.

(24) Boero, M.; Terakura, K.; Ikeshoji, T.; Liew, C. C.; Parrinello, M. *J. Chem. Phys.* **2001**, *115*, 2219.

(25) Kalinichev, A. G.; Churakov, S. V. *Fluid Phase Equilbr.* **2001**, 183−184, 271.

(26) Johansson, E.; Bolton, K.; Ahlstrom, P. *J. Chem. Phys.* **2005**, *123*, 024504.

(27) Liu, K.; Cruzan, J. D.; Saykally, R. J. *Science* **1996**, *271*, 929.
(28) Swope, W. C.; Andersen, H. C.; Berens, P. H.; Wilson, K. R. *J. Chem. Phys.* **1982**, *76*, 637.
(29) Dunn, M. E.; Pokon, E. K.; Shields, G. C. *J. Am. Chem. Soc.* **2004**, *126*, 2647.
(30) Berendsen, H. J. C.; Postma, J. P. M.; van Gunsteren, W. F.; Hermans, J. In *Intermolecular Forces*; Pullmann, B., Ed.; D. Reidel: Dordrecht, The Netherlands 1981; p 331.
(31) Berendsen, H. J. C.; Grigera, J. R.; Straatsma, T. P. *J. Phys. Chem.* **1987**, *91*, 6269.
(32) Boulougouris, G. C.; Economou, I. G.; Theodorou, D. N. *J. Phys. Chem. B* **1998**, *102*, 1029.
(33) Jorgensen, W. L.; Chandrasekhar, J.; Madura, J. D.; Impey, R. W.; Klein, M. L. *J. Chem. Phys.* **1983**, *79*, 926.
(34) Jorgensen, W. L.; Madura, J. D. *Mol. Phys.* **1985**, *56*, 1381−1392.